2019

Fiber element simulation of interaction behavior of local and global buckling in axially loaded rectangular concrete-filled steel tubular slender columns under fire exposure

Ghanim Mohammed Kamil
Victoria University

Qing Quan Liang
Victoria University, qing.liang@vu.edu.au

Muhammad N. S Hadi
University of Wollongong, mhadi@uow.edu.au

Fiber element simulation of interaction behavior of local and global buckling in axially loaded rectangular concrete-filled steel tubular slender columns under fire exposure

Abstract

Slender rectangular thin-walled concrete-filled steel tubular (CFST) columns in composite building structures exposed to fire may experience the interaction of local and global buckling. Numerical investigations on the interaction buckling responses of such columns under fire exposure have been rarely reported. This paper describes a fiber-based computational model for the prediction of the fire-resistance and interaction responses of local and global buckling of concentrically-loaded slender CFST columns made of rectangular sections exposed to fire. The thermal analysis is undertaken to calculate the distribution of temperatures in the column cross-section considering the effects of the air gap between concrete and steel, exposure surface emissivity as well as moisture content in concrete. The local and post-local buckling models proposed previously for steel tube walls at elevated temperatures are incorporated in the inelastic analysis of cross-sections to model the progressive post-local buckling. The global buckling analysis of slender CFST columns exposed to fire accounts for the effects of material and geometric nonlinearities as well as local buckling. Efficient computational procedure and solution algorithms are developed to solve the nonlinear equilibrium dynamic functions of loaded slender CFST columns exposed to fire. Independent experimental and numerical results on slender CFST columns are utilized to validate the computational model. The interaction behavior of local and global buckling and fire-resistance of slender rectangular CFST columns are investigated. It is shown that the developed computational model provides a reasonably accurate and efficient method for the prediction of the interaction buckling responses as well as the fire-resistance of slender CFST columns subjected to axial loading and fire.

Keywords

behavior, interaction, element, fiber, simulation, exposure, columns, slender, under, tubular, axially, fire, steel, concrete-filled, buckling, global, local, loaded, rectangular

Disciplines

Engineering | Science and Technology Studies

Publication Details

Kamil, G. Mohammed., Liang, Q. Quan. & Hadi, M. N. S. (2019). Fiber element simulation of interaction behavior of local and global buckling in axially loaded rectangular concrete-filled steel tubular slender columns under fire exposure. Thin-Walled Structures, 145 106403-1-106403-15.

Revised manuscript prepared for

Thin-Walled Structures

July 2019

Fiber element simulation of interaction behavior of local and global buckling in axially loaded rectangular concrete-filled steel tubular slender columns under fire exposure

Ghanim Mohammed Kamil[a], Qing Quan Liang[a,*], Muhammad N. S. Hadi[b]

[a] College of Engineering and Science, Victoria University, PO Box 14428, Melbourne, VIC 8001, Australia
[b] School of Civil, Mining and Environmental Engineering, University of Wollongong, Wollongong, NSW 2522, Australia

Corresponding author:

Dr Qing Quan Liang
College of Engineering and Science
Victoria University
PO Box 14428
Melbourne VIC 8001
Australia
E-mail: Qing.Liang@vu.edu.au

Fiber element simulation of interaction behavior of local and global buckling in axially loaded rectangular concrete-filled steel tubular slender columns under fire exposure

Ghanim Mohammed Kamil[a], Qing Quan Liang[a,*], Muhammad N. S. Hadi[b]

[a] *College of Engineering and Science, Victoria University, PO Box 14428, Melbourne, VIC 8001, Australia*

[b] *School of Civil, Mining and Environmental Engineering, University of Wollongong, Wollongong, NSW 2522, Australia*

Abstract

Slender rectangular thin-walled concrete-filled steel tubular (CFST) columns in composite building structures exposed to fire may experience the interaction of local and global buckling. Numerical investigations on the interaction buckling responses of such columns under fire exposure have been rarely reported. This paper describes a fiber-based computational model for the prediction of the fire-resistance and interaction responses of local and global buckling of concentrically-loaded slender CFST columns made of rectangular sections exposed to fire. The thermal analysis is undertaken to calculate the distribution of temperatures in the column cross-section considering the effects of the air gap between concrete and steel, exposure surface emissivity as well as moisture content in concrete. The local and post-local buckling models proposed previously for steel tube walls at elevated temperatures are incorporated in the inelastic analysis of cross-sections to model the progressive post-local buckling. The global buckling analysis of slender CFST columns exposed to fire accounts for the effects of material

* Corresponding author.
E-mail address: Qing.Liang@vu.edu.au (Q. Q. Liang)

and geometric nonlinearities as well as local buckling. Efficient computational procedure and solution algorithms are developed to solve the nonlinear equilibrium dynamic functions of loaded slender CFST columns exposed to fire. Independent experimental and numerical results on slender CFST columns are utilized to validate the computational model. The interaction behavior of local and global buckling and fire-resistance of slender rectangular CFST columns are investigated. It is shown that the developed computational model provides a reasonably accurate and efficient method for the prediction of the interaction buckling responses as well as the fire-resistance of slender CFST columns subjected to axial loading and fire.

Keywords: Concrete-filled steel tubes; Elevated temperatures; Fire-resistance; Nonlinear analysis; Interaction of local and global buckling.

1. Introduction

Thin-walled square and rectangular concrete-filled steel tubular (CFST) slender columns as illustrated in Fig. 1 have been used widely in subway stations, bridges, industrial buildings and tall buildings to support heavy loads [1]. The CFST columns possess not only high strength, stiffness, ductility and seismic resistance but also high fire-resistance. The behavior of short and slender CFST columns at room temperatures has been investigated experimentally and numerically by researchers [2-8]. In design codes [9], a column having a member slenderness ratio (L/r) greater than 22 is treated as a slender column, where L is the column effective length and r denotes the radius of gyration of its cross-section. The design of slender CFST columns for the fire limit state is one of the important design criteria that must be considered in practice [10]. To achieve economical designs, thin-walled steel tubes are often used to construct rectangular CFST columns. However, slender rectangular CFST columns where steel cross-

sections are non-compact or slender exposed to fire may undergo the interaction of local and global buckling, which is complex and has not been fully understood [6, 11]. Although fire tests on such composite columns can be conducted, they are highly expensive and time-consuming. Computer simulation programs are cost-effective numerical techniques that compute the fire-resistance of CFST columns. However, computational research on the interaction of local and global buckling of rectangular CFST slender columns exposed to fire has been extremely limited [12]. Therefore, an efficient computer simulation model for the prediction of concentrically loaded rectangular slender CFST columns exposed to fire considering coupled instability is much needed.

When CFST columns in engineering structures are exposed to fire, they are subjected to constant axial or eccentric loads. The behavior of a CFST column during various stages of the fire exposure can be described as follows: (1) in the initial phase, the temperature of the steel section rises rapidly and the column load is mainly carried by the steel tube; (2) when the temperature of the steel tube is high enough, the stiffness and resistance of the tube reduce considerably and the load of the column is transferred to the concrete core; (3) during this development, the axial and bending stiffness of the composite section are reduced due to the local buckling of the steel tube, leading to rapidly growing lateral displacement of the column. Standard fire tests have been conducted to determine the fire-responses of loaded CFST slender columns under increasing temperatures by researchers [13-21]. The axial and lateral deformations, temperatures on the column, and fire-resistance were measured in a standard fire test. Lie and Chabot [13] and Kodur and Lie [15] performed fire tests on the fire responses of circular and square CFST slender columns made of plain or reinforced concrete under axial loads. The influences of sectional dimension, section type, column slenderness, applied load ratio, and loading eccentricity on the fire behavior were examined. Square columns had the

length of 3810 mm and the width-to-thickness ratios ranging from 24 to 48. It was observed that slender square CFST columns failed by the interaction of local and global buckling. Han et al. [16] undertook experiments on the fire-performance of CFST columns made of square and rectangular sections with and without fire protection loaded either axially or eccentrically. It was reported that the fire resistance of CFST columns was moderately affected by the material strengths, steel ratio and load eccentricity, but significantly influenced by the cross-sectional area, protection thickness and column slenderness. Moreover, the interaction of local and global buckling caused the failure of slender columns.

Experimental results on seven square CFST slender columns loaded axially and subjected to increasing temperatures were reported by Kim et al. [17]. The tested columns had the width-to-thickness ratios of 33.3 and 38.9 and a length of 3500 mm. However, only part of the column length was heated in the furnace. Espinos et al. [18] performed tests to examine the influences of large loading eccentricities on the fire-resistance of slender CFST columns constructed by circular or square sections reinforced with steel bars. Test results showed that square columns failed by global buckling due to their small width-to-thickness ratios of 18.75 and 22. In addition, the fire resistance of CFST columns was remarkably reduced by increasing the loading eccentricity. Espinos et al. [19] undertook further tests on the fire behavior of slender CFST columns of rectangular and elliptical sections loaded concentrically or eccentrically. The aforementioned fire tests have shown that loaded slender thin-walled CFST rectangular columns with the width-to-thickness ratios of 15, 25 and 35 exposed to fire failed by the interaction local and global buckling. The load was transferred from the buckled steel tube to the concrete core, which caused the crushing of concrete.

Researchers have employed the nonlinear computational procedures to investigate the responses of slender CFST columns subjected to standard fire defined by the standard temperature-time curve [22-32]. A mathematical model using the fiber approach was proposed by Lie and Irwin [23] for computing the temperature distributions as well as the load-deflection behavior of CFST rectangular columns with longitudinal reinforcing bars subjected to concentric loads and elevated temperatures. The thermal analysis considered the effect of water content in the concrete. However, the tensile behavior of concrete, deflection caused by preload and the interaction of local and global buckling were not taken into account in the mathematical model. Han [24] developed a fiber-based numerical model to determine the fire-resistance as well as the strength of slender CFST beam-columns of square and circular sections loaded eccentrically. The temperature fields in column cross-sections were calculated by the finite element method. The numerical model by Han [24] has not incorporated the interaction of local and global buckling and the deformations induced by preloads in the fire-resistance simulations of slender square CFST columns. The fire-performance of slender square CFST columns subjected to either concentric or eccentric loads was investigated by Chung et al. [25, 26] by employing the fiber-based numerical models. The limitations of their numerical models are that the models have not considered the effects of local buckling, initial geometric imperfection and air gap at the concrete-steel interface on the fire responses.

Renaud et al. [27] developed a finite element (FE) model for simulating the behavior of slender CFST columns considering the interaction between the concrete and steel tube, and geometric and material nonlinearities. It was reported that the FE model predicted well the fire resistance with good accuracy. Yang et al. [28] proposed a fiber-based FE model for determining the post-fire responses of square and circular CFST slender columns that were eccentrically loaded after being exposed to standard fire. The limitations of their model were that it did not incorporate

the effects of tensile concrete behavior and local buckling. A fiber-based FE beam-column model was developed by Ibanez et al. [29] for the predictions of the fire performance of circular CFST slender columns loaded concentrically to failure. The gap conductance at the concrete-steel interface and the initial deflection of columns were considered in the model. It was shown that the FE model generally predicted well the measured fire responses of circular CFST slender columns but could not be able to capture the responses at the last stages of fire exposure.

Ding and Wang [30] and Espinos et al. [31] used commercial finite-element programs to determine the effects of the air-gap and slip between the steel tube and concrete as well as concrete tensile strength on the fire performance of loaded slender CFST square columns with initial geometric imperfections. It was found that the effect of the slip between the steel and concrete on the fire behavior was minor while the inclusion of an air gap improved the accuracy of numerical simulations. Hong and Varma [32] developed a sequentially coupled FE model using ABAQUS to determine the fire behavior of slender CFST square columns. The FE model was used to examine the sensitivities of the fire performance of CFST columns to local buckling, geometric imperfections, and material constitutive models. The numerical results confirmed that the stress-strain models for concrete and steel at high temperatures had marked effects on the predicted fire responses. However, it was found that the cracking behavior of concrete in tension could not be accurately simulated by the FE model.

The above literature review shows that the fiber-based numerical models presented by other researchers have not considered the effects of the interaction of local and global buckling, deformations caused by the preload, and initial geometric imperfections on the fire responses of CFST rectangular columns loaded concentrically. The finite element models developed using commercial programs might include the aforementioned important features, but their

computational cost is very expensive compared to the fiber-based numerical models. The local buckling has been considered in the fiber-based model proposed by Kamil et al. [12] for the fire response analysis of rectangular short CFST columns but has not been included in the global buckling simulation of rectangular CFST slender columns that are loaded concentrically.

This paper presents a mathematical model underlying the theory of fiber analysis for the simulation of slender CFST columns of rectangular sections exposed to standard fire loading considering the interaction of local and global buckling, deformations caused by the preload, and initial geometric imperfections. The theoretical formulation, computer simulation procedure and numerical solution algorithms for computing the ultimate strength and fire-resistance of slender CFST columns accounting for material and geometric nonlinearities at elevated temperatures are described. The independent experimental and numerical results are employed to validate the numerical model. The responses due to the interaction of local and global buckling of CFST rectangular columns under fire are investigated by using the developed computational model.

2. Cross-sectional analysis incorporating local buckling

2.1. Discretization of cross-section

The cross-section of a rectangular CFST column is divided into fiber elements by using the fiber element approach [5, 11, 33]. A typical fiber mesh used for both the stress and thermal analyses is illustrated in Fig. 2, where the size of the steel fiber is half of that of the concrete fiber. However, the discretization of the column along its length is not required in the fiber approach, which significantly reduces the computational time in comparison with the finite

element method. Both the mechanical and thermal properties are assigned to steel and concrete fibers. In the thermal analysis, temperatures at the nodes of fiber elements are computed. The temperature at an element is taken as the average temperature at its nodes. Stresses at fibers are calculated from axial strains by means of using the uniaxial temperature-dependent stress-strain models for steel and concrete.

The assumptions made in the formulation of the mathematical model are: (1) the rectangular CFST slender column is subjected to uniform temperatures along its length; (2) there is no slippage between the concrete infill and steel tube in the longitudinal direction; (3) after deformation, the plane section remains plane; (4) the effects of local and post-local buckling of thin-walled steel tubes are included; (5) an air gap between the concrete core and steel tube is considered; (6) the concrete tensile strength is ignored; (7) the shrinkage and creep of concrete are not taken into account.

2.2. Temperature distributions

The calculations of temperatures on a rectangular CFST column exposed to fire involve the determinations of temperatures on its outer surfaces and temperatures within its cross-section. The temperatures on the column surfaces are computed by using the standard temperature-time relationship provided in Eurocode 1 [34], which is written as

$$T(t) = 20 + 345log_{10}(8t + 1) \tag{1}$$

in which T represents the temperature in ^{o}C and t stands for the fire exposure time in minutes.

The distribution of temperatures within the column cross-section is determined by means of solving the following heat equation [35]:

$$k\frac{\partial^2 T}{\partial x^2}+k\frac{\partial^2 T}{\partial y^2}+q=\rho c\frac{\partial T}{\partial t} \tag{2}$$

where the density ρ is in kg/m^3, c denotes the specific heat in J/kg, k represents the thermal conductivity in $\mathrm{W/m^oC}$ and q stands for the heat flux. The concrete properties at elevated temperatures provided by Lie and Chabot [22] and the steel properties at elevated temperatures specified in Eurocode 3 [36] are used in the present mathematical model and details can also be found in the paper by Kamil et al. [12].

The heat equation in 2D space with time expressed by Eq. (2) is solved by means of employing the finite difference method. The nodal temperatures of fiber elements as illustrated in Fig. 3 are computed by the forward finite difference method of the heat equation expressed by

$$T_{m,n}^{i+1}=\frac{\alpha\Delta t}{(\Delta L)^2}\left(T_{m,n-1}^{i}+T_{m,n+1}^{i}+T_{m-1,n}^{i}+T_{m+1,n}^{i}\right)+\left(1-\frac{4\alpha\Delta t}{(\Delta L)^2}\right)T_{m,n}^{i} \tag{3}$$

where $1-(4\alpha\Delta t/\Delta L)^2\geq 0$; $\alpha=k/\rho c$; Δt stands for the time increment in seconds; and the element length is $\Delta L=dx=dy$.

Ding and Wang [30] reported that the predictions of structural and thermal responses of CFST columns were found to improve by introducing an air gap between the concrete and steel tube. Therefore, such an air gap is included in the temperature calculations in which the thermal

contact resistance (h_{tr}) of 100 W/m^2K is specified for the air gap as suggested by Ding and Wang [30]. In the present formulation, a constant value of 0.7 is adopted for the emissivity of exposed surfaces ($\hat{\varepsilon}$), the Stephan-Boltzmann constant is taken as 5.67×10^{-8} W/m^2K^4, and the moisture content of 3% is used [30, 37]. The numerical model assumes that when the temperature of the fiber element reaches 100°C, the moisture in concrete starts to evaporate until the fiber element is dry. All the heat supplied to the fiber clement during the period of evaporation is utilized for the evaporation of moisture as suggested by Lie and Irwin [23]. By taking the effects of the air gap into account, the temperatures at the contact nodes at the corner of the steel-concrete interface as depicted in Fig. 4 are calculated by

$$T_{1,1}^{i+1} = T_{1,1}^{i} + \frac{4\Delta t}{\rho c d_c^2}\left[h_{tr}(T_{3,3}^{i} - T_{1,1}^{i})d_c + \lambda_c(T_{1,2}^{i} - T_{1,1}^{i}) + \lambda_c(T_{2,1}^{i} - T_{1,1}^{i})\right] \quad (4)$$

in which $T_{1,1}$ is the nodal temperature at the node of the corner concrete fiber; $T_{1,2}$ and $T_{2,1}$ are the nodal temperatures of the concrete fiber nodes adjacent to the corner respectively; $T_{3,3}$ is the nodal temperature of the corner node of the steel fiber; d_c denotes the size of concrete fibers; λ_c is the thermal conductivity of concrete as a function of the averaged temperature of two adjacent nodes [12, 38]. Equation (4) is used to compute the nodal temperatures at fibers at the boundaries with the thermal radiation and heat convection coefficients. The numerical model proposed for the thermal analysis has been verified by comparisons with experimental data as well as numerical solutions by Kamil et al. [12].

2.3. Strain distribution

The linear strain distribution in the column cross-section is shown in Fig 2, where ε_m is the strain at the extreme compressive fiber. As demonstrated in Fig. 2, the strain at any fiber is determined by multiplying the curvature by the distance measured from the element centroid to the neutral axis. In the analysis, compressive strains are treated as positive and tensile strains as negative. For a CFST slender column with rectangular section subjected to concentric loading, the column will buckle about the weak axis. The fiber strains are calculated as follows:

$$y_{n,i} = \frac{D}{2} - d_n \tag{5}$$

$$d_{e,i} = | y_i - y_{n,i} | \tag{6}$$

$$\varepsilon_i = \begin{cases} \phi d_{e,i} - \varepsilon_T & \text{for } y_i \geq y_{n,i} \\ -\phi d_{e,i} - \varepsilon_T & \text{for } y_i < y_{n,i} \end{cases} \tag{7}$$

where d_n denotes the distance of the neutral axis from the edge fiber in the composite section, $d_{e,i}$ represents the perpendicular distance from the neutral axis to the centroid of each element, y_i stands for coordinates of the fiber i, ε_i denotes the strain of the element i; ϕ represents the curvature; and ε_T is the thermal strain of steel or concrete [12].

2.4. Modeling of critical local buckling

Elevated temperatures cause a significant reduction in the steel tube stiffness and strength of a CFST column with rectangular sections subjected to axial compression and bending. This increases the possibility of the local buckling of steel plates [10, 12]. Expressions for determining the critical local-buckling stresses of steel tube walls of CFST rectangular columns subjected to non-uniform stresses at elevated temperatures were proposed by Kamil et al. [39].

These expressions accounted for the residual stresses in the steel plates at temperatures below 400°C and initial geometric imperfection and can be applied to plates having clear width-to-thickness ratios (b/t_s) in the range of 30 to 110. The formulas derived by Kamil et al. [39] are utilized in the proposed computational procedures to calculate the critical local-buckling stresses of steel tube walls in rectangular CFST slender columns under fire. For temperatures from 550 to 650°C, the critical local buckling stress of plates [39] is calculated by

$$\frac{\sigma_{1c,T}}{f_{y,T}} = \left(0.1916\lambda_{c,T}^{-0.7661} + 0.003889\right)\left(m_1\lambda_{c,T}^2 + m_2\lambda_{c,T} + m_3\right) \tag{8}$$

where $\sigma_{1c,T}$ is the critical local-buckling stress of plate at elevated temperatures, $f_{y,T}$ is the temperature-dependent steel yield stress, and $\lambda_{c,T}$ represents the temperature-dependent relative slenderness of a steel plate, written as

$$\lambda_{c,T} = \sqrt{\frac{12(1-\nu^2)(b/t_s)^2(R_{y,T}f_y)}{k\pi^2(R_{E,T}E)}} \tag{9}$$

In Eq. (9), f_y is the steel yield strength at room temperature, ν is the Poisson's ratio of steel, E is the Young's modulus of steel at room temperature, $k = 9.95$ is the elastic local buckling coefficient of steel plates with clamped boundary conditions as reported by Liang et al. [40]. The parameters $R_{y,T}$ and $R_{E,T}$ are reduction factors applied to the steel yield strength and Young's modulus due to elevated temperatures, respectively, and are given in Eurocode 3 [36] and shown in Fig. 5.

The coefficients m_1, m_2 and m_3 in Eq. (8) are determined from

$$m_1 = -1.0685\alpha_s^2 + 2.275\alpha_s - 0.8969 \tag{10}$$

$$m_2 = 2.3075\alpha_s^2 - 4.7791\alpha_s + 1.8475 \tag{11}$$

$$m_3 = -0.825\alpha_s^2 + 1.086\alpha_s + 1.0083 \tag{12}$$

where the coefficient of stress gradient α_s is determined as the ratio of the minimum edge stress to the maximum edge stress on the plate.

For any other temperatures, Kamil et al. [39] proposed the following equation for the determination of the critical local buckling stresses of steel plates:

$$\frac{\sigma_{1c,T}}{f_{y,T}} = (g_1\lambda_{c,T}^{g} + g_2)\frac{0.6566\lambda_{c,T}^{0.001521}\left(\frac{R_{p,T}}{R_{y,T}}\right)^{-0.1598}}{0.5415\lambda_{c,T}^{4.889} + \left(\frac{R_{p,T}}{R_{y,T}}\right)^{-0.8252}} \tag{13}$$

where $R_{p,T}$ is the reduction factor to the proportional limit $f_{p,T}$ given in Fig. 5, and the coefficients g, g_1 and g_2 are expressed as

$$g = -7.9339\alpha_s^2 + 11.29\alpha_s + 4.701 \tag{14}$$

$$g_1 = 0.0863\alpha_s^2 - 0.1248\alpha_s + 0.0431 \tag{15}$$

$$g_2 = 0.2656\alpha_s^2 - 0.9902\alpha_s + 1.719 \tag{16}$$

2.5. Modeling of post-local buckling

The effective width method can be employed to calculate the post-local buckling strengths of steel plates in CFST columns with rectangular sections as discussed by Liang [11] and Liang et al. [40]. The effective width equations were given by Kamil et al. [39] for steel tube walls of CFST rectangular columns at any temperatures. Figure 5 illustrates the ineffective and effective widths of a rectangular steel cross-section subjected to axial compression as well as uniaxial bending. The present fiber technique incorporates the following expressions of effective width by Kamil et al. [39] to model the post-local buckling of slender CFST columns exposed to fire:

$$\frac{b_{e1}}{b}=\frac{1}{2}(q_1\lambda_{c,T}^{q})\frac{0.8418\lambda_{c,T}^{0.02368}\left(\frac{R_{p,T}}{R_{y,T}}\right)^{-0.3028}+1.154\left(\frac{R_{p,T}}{R_{y,T}}\right)}{2.055+\lambda_{c,T}^{1.68}} \qquad (\alpha_s=1.0) \tag{17}$$

$$\frac{b_{e1}}{b}=\frac{1}{3}(q_1\lambda_{c,T}^{q})\frac{0.8418\lambda_{c,T}^{0.02368}\left(\frac{R_{p,T}}{R_{y,T}}\right)^{-0.3028}+1.154\left(\frac{R_{p,T}}{R_{y,T}}\right)}{2.055+\lambda_{c,T}^{1.68}} \qquad (\alpha_s=0) \tag{18}$$

$$\frac{b_{e2}}{b}=(2-\alpha_s)\frac{b_{e1}}{b} \tag{19}$$

where b_{e1} and b_{e2} denote the effective widths depicted in Fig. 6, b is the clear width of the steel plate, q and q_1 are expressed as

$$q=0.04007\alpha_s^2-0.05275\alpha_s+0.03355 \tag{20}$$

$$q_1=0.1007\alpha_s^2-0.7027\alpha_s+1.65 \tag{21}$$

The progressive post-local buckling behavior of a thin steel plate is developed due to the gradual redistribution of in-plane stresses in the buckled plate. The numerical scheme for simulating

the progressive post-local buckling proposed by Liang [5] is implemented in the present computational model. The full details of the scheme can be found in the work by Liang [5, 11].

2.6. Axial force and bending moment

The internal axial force (P) and bending moment (M_x) in the cross-section of a CFST rectangular column under combined axial compression and uniaxial bending are computed as stress resultants by the following equations:

$$P = \sum_{j=1}^{ns} \sigma_{s,j} A_{s,j} + \sum_{k=1}^{nc} \sigma_{c,k} A_{c,k} \tag{22}$$

$$M_x = \sum_{j=1}^{ns} \sigma_{s,j} A_{s,j} y_j + \sum_{j=1}^{nc} \sigma_{c,k} A_{c,k} y_k \tag{23}$$

in which subscripts j and k denotes the fibers in the concrete and steel tube, respectively; subscripts s and c represent steel and concrete, respectively; σ is the longitudinal fiber stress; A denotes the area of a fiber element; y is the coordinate of the fiber element; nc and ns are the total element numbers in the concrete and steel tube, respectively.

3. Global buckling analysis

3.1. Theoretical formulation

A mathematical model is formulated for the global buckling analysis of concentrically-loaded CFST rectangular columns exposed to fire. Both ends of the slender column are pin-supported. The concentrically-loaded slender column at elevated temperatures is subjected to single

curvature bending about its minor principal axis. The half-sine wave shape function has been used by a number of researchers and shown to predict well the deformed shape of pin-ended slender columns [41-44]. Therefore, the half-sine wave shape function is used to model the column deformed shape, which is expressed by

$$u = u_m \sin\left(\frac{\pi z}{L}\right) \tag{24}$$

in which u_m denotes the lateral displacement at the mid-length of the column, and L represents the column effective length.

The curvature at the column mid-length can be determined from the displacement function as

$$\phi_m = u_m \left(\frac{\pi}{L}\right)^2 \tag{25}$$

The constant axial load acting on the CFST column before being exposed to fire induces initial stresses and deflections within the column. This constant axial load is treated as a preload on the column as suggested by Patel et al. [44]. The mid-height lateral deflection caused by the preload is calculated using the load-deflection computational procedure and is used as an additional initial geometric imperfection (u_{po}) in the fire-resistance simulation. The initial geometric imperfection (u_o) and lateral displacement (u_m) at the column mid-length are also included in the formulation. The external bending moment at the column mid-length is therefore

$$M_{ext} = P(u_{po} + u_o + u_m) \tag{26}$$

To determine the complete axial load-lateral deflection responses of slender CFST columns exposed to fire, the method of deflection control is adopted in the formulation. The lateral deflection at the column mid-length is incremented in steps. The method calculates the axial load on the column that causes the given lateral displacement. The internal axial force in the column satisfying the moment equilibrium at the mid-height is treated as the external applied axial load. The complete axial load-lateral displacement responses of the slender CFST column are determined by means of repeating this computational procedure. The residual moment function in the calculation is expressed as

$$r_M = M_x - P(u_{po} + u_o + u_m) \tag{27}$$

The moment equilibrium condition is achieved if $|r_M| < \varepsilon_k = 10^{-4}$ in the numerical calculations.

3.2. Numerical solution algorithms

To determine the true internal axial force corresponding to a specified lateral deflection, the neutral axis depth (d_n) needs to be iteratively adjusted. It should be noted that the residual moment function is a dynamic nonlinear function which is not derivative with respect to the design available. Therefore, Muller's method [45] is utilized to determine the neutral axis depth in the cross-section [6, 33, 43]. The method requires three initial neutral axis depths $d_{n,1}$, $d_{n,2}$ and $d_{n,3}$ to begin the iterative computation process. The new neutral axis depth $d_{n,4}$ is calculated by means of applying the following equations:

$$d_{n,4} = d_{n,3} + \frac{-2c_m}{b_m \pm \sqrt{b_m^2 - 4a_m c_m}} \tag{28}$$

$$a_m = \frac{(d_{n,2} - d_{n,3})(r_{M,1} - r_{M,3}) - (d_{n,1} - d_{n,3})(r_{M,2} - r_{M,3})}{(d_{n,1} - d_{n,2})(d_{n,1} - d_{n,3})(d_{n,2} - d_{n,3})} \quad (29)$$

$$b_m = \frac{(d_{n,2} - d_{n,3})^2(r_{M,2} - r_{M,3}) - (d_{n,2} - d_{n,3})^2(r_{M,1} - r_{M,3})}{(d_{n,1} - d_{n,2})(d_{n,1} - d_{n,3})(d_{n,2} - d_{n,3})} \quad (30)$$

$$c_m = r_{M,3} \quad (31)$$

The above equations are employed to iteratively adjust the location of the neutral axis until the condition of moment equilibrium is satisfied.

3.3. Computational procedure

A sequential coupled computational procedure is developed to determine the ultimate axial resistance and fire-resistance of concentrically-loaded slender CFST rectangular columns exposed to fire, including the influences of interaction of local and global buckling. For a given fire exposure time, the column ultimate axial strength is determined by employing the method of load-deflection analysis [42]. The computation is repeated until the complete ultimate axial load-fire exposure time curve is obtained. The ultimate axial load of the CFST slender column decreases gradually as the fire exposure time increases. The fire exposure time for reaching the failure point in the load-displacement curve of the CFST column is the computed fire resistance. The computer flow chart for calculating the ultimate axial strength and fire-resistance of a loaded CFST column exposed to standard fire is depicted in Fig. 7 and the main computational steps are described as follows:

1. Input data.
2. Divide the column cross-section into fine fibers.
3. Compute the lateral deformation of the slender column under constant axial load.

4. Initialize the fire exposure time as $t = \Delta t$.
5. Calculate temperatures on column surfaces and at fiber elements in its cross-section.
6. Initialize the lateral displacement at the column mid-length as $u_m = \Delta u_m$.
7. Calculate the curvature ϕ_m at the column mid-length.
8. Adjust the neutral axis depth d_n using Müller's method.
9. Calculate element stresses from strains using the temperature-dependent stress-strain models for steel and concrete.
10. Simulate the initial local and post-local buckling behavior of the steel tube walls.
11. Determine the internal axial force *P* and moment M_x.
12. Compute the residual moment function r_M.
13. Repeat Steps 8 to 12 until $|r_M| < \varepsilon_k = 10^{-4}$.
14. Increase the mid-height deflection by $u_m = u_m + \Delta u_m$.
15. Repeat Steps 7 to 14 until $P < 0.5P_u$ or the deflection exceeds the specified limit (u_l).
16. Increase the fire exposure time by $t = t + \Delta t$.
17. Repeat Steps 5 to 16 until the fire-resistance of the CFST column is obtained.

4. Constitutive relationships for materials at elevated temperatures

4.1. Structural steels

The temperature-dependent stress-strain relations of structural steels given in Eurocode 3 [36] is implemented in the computational algorithms developed. The stress-strain relations of steels as a function of temperatures are plotted in Fig. 8, and are determined by:

$$\sigma_{s,T}=\begin{cases} E_T\varepsilon_s & \text{for } \varepsilon_s \le \varepsilon_{p,T} \\ \left(f_{p,T}-h_3\right)+\dfrac{h_2}{h_1}\sqrt{h_1^{\,2}-\left(\varepsilon_{y,T}-\varepsilon_s\right)^2} & \text{for } \varepsilon_{p,T} < \varepsilon_s \le \varepsilon_{y,T} \\ f_{y,T} & \text{for } \varepsilon_{y,T} < \varepsilon_s \le \varepsilon_{t,T} \\ f_{y,T}\left[1-\left(\varepsilon_s-\varepsilon_{t,T}\right)/\left(\varepsilon_{u,T}-\varepsilon_{t,T}\right)\right] & \text{for } \varepsilon_{t,T} < \varepsilon_s \le \varepsilon_{u,T} \\ 0 & \text{for } \varepsilon_s > \varepsilon_{uT} \end{cases} \tag{32}$$

where

$$h_1^{\,2}=(\varepsilon_{y,T}-\varepsilon_{p,T})(\varepsilon_{y,T}-\varepsilon_{p,T}+h_3/E_T) \tag{33}$$

$$h_2^{\,2}=E_T(\varepsilon_{y,T}-\varepsilon_{p,T})h_3+h_3^{\,2} \tag{34}$$

$$h_3=\frac{(f_{y,T}-f_{p,T})^2}{E_T\,(\varepsilon_{y,T}-\varepsilon_{p,T})-2\,(f_{y,T}-f_{p,T})} \tag{35}$$

in which E_T is the temperature-dependent Young's modulus for the steel, $\varepsilon_{p,T}$ is the strain at the proportional limit $f_{p,T}$, $\varepsilon_{y,T}$ is the yield strain, and $\varepsilon_{u,T}$ is the temperature-dependent ultimate strain.

Structural steels exhibit strain-hardening at temperatures below $400^{o}\mathrm{C}$, which is considered in the formulation by [36]:

$$\sigma_{s,T}=\begin{cases} 50\left[\left(f_{u,T}-f_{y,T}\right)/0.02\right]+2\,f_{y,T}-f_{u,T} & \text{for } 0.02<\varepsilon_s \le 0.04 \\ f_{u,T} & \text{for } 0.04<\varepsilon_s \le 0.15 \\ f_{u,T}\left[1-20\left(\varepsilon_s-0.15\right)\right] & \text{for } 0.15<\varepsilon_s \le 0.2 \end{cases} \tag{36}$$

in which $f_{u,T}$ is the temperature-dependent tensile strength of steel, which is computed by

$$f_{u,T} = \begin{cases} f_u R_{y,T} & \text{for } T \le 300^o C \\ f_{y,T} + 0.01\left(f_{u,T} - f_{y,T}\right)(400 - T) & \text{for } 300 < T \le 400^o C \end{cases} \quad (37)$$

4.2. Concrete

Experiments indicated that the rectangular steel tube provides little confinement to the concrete core in a rectangular CFST column and the confinement is limited to the corers, which does not increase the compressive strength of concrete but improves the ductility of the concrete [5, 6, 11]. In addition, high temperature and local buckling significantly reduce the strength and stiffness of the rectangular steel tube, which provides no confinement to the concrete core so that it is neglected in the present study. Eurocode 2 [37] provides a temperature-dependent stress-strain model for concrete, which is adopted in the proposed computational procedure. Figure 9 depicts the stress-strain-curves as a function of temperatures determined by means of applying the model given in Eurocode 2. These curves are expressed by

$$\sigma_{c,T} = \begin{cases} \dfrac{3\varepsilon_c f'_{c,T}}{\varepsilon'_{c,T}\left[2 + \left(\varepsilon_c / \varepsilon'_{c,T}\right)^3\right]} & \text{for } \varepsilon_c \le \varepsilon'_{c,T} \\ f'_{c,T}\left[\dfrac{\varepsilon_{cu,T} - \varepsilon_c}{\varepsilon_{cu,T} - \varepsilon'_{c,T}}\right] & \text{for } \varepsilon_c > \varepsilon'_{c,T} \end{cases} \quad (38)$$

where $f'_{c,T}$ denotes the concrete compressive strength, $\varepsilon'_{c,T}$ represents the concrete strain at $f'_{c,T}$, and $\varepsilon_{cu,T}$ is the temperature-dependent ultimate concrete strain. The values of $\varepsilon'_{c,T}$ and $\varepsilon_{cu,T}$ for concrete with siliceous aggregates are given in Eurocode 2 [37].

5. Verification of the fiber-based computational model

The test and computational results on the fire-resistance of loaded slender CFST square and rectangular columns made of plain concrete reported by Lie and Chabot [13], Kim et al. [17], Han [24], Chung et al. [26], and Ding and Wang [30] were utilized to validate the proposed computational model. These columns had the dimensions and ambient temperature material properties given in Table 1, where the effective lengths of these columns and the applied constant axial loads are also shown. The local buckling was included in the global buckling simulations for cross-sections with the b / t_s ratio greater than 30.

The tested fire-resistance times of CFST columns with square sections reported by Lie and Chabot [13] and Kim et al. [17] are compared with predictions by the fiber-based analysis procedure in Fig. 10. It is demonstrated that there are reasonably good correlations between predictions and test data. The computational model generally produces conservative fire-resistance of tested columns. As shown in Fig. 10, most of the predicted results are on the safe side. The discrepancy between tested and computed fire-resistance is likely due to the uncertainties in the steel and concrete properties at elevated temperatures and water contents in concrete. Particularly, the concrete properties and water contents in the actual specimens are unknown. Moreover, in the standard fire test, only part of the column length was exposed to fire. This implies that the measured fire-resistance time of the column is generally longer than the computed result.

The axial load-lateral displacement curves for a slender square CFST column during various fire-exposure times determined by the present computational program and the numerical model given by Han [24] are compared in Fig. 11, where P_{uo} is the ultimate axial strength of the

column at ambient temperature. It appears that both numerical models produce almost the same load-deflection curve for the column at ambient temperature. However, the load-deflection curve at elevated temperatures given by Han slightly differs from the one simulated by the present computational model. The reason for this is that both numerical models employed different temperature-dependent material constitutive laws for steel and concrete. As demonstrated in Fig. 12, the ultimate axial strengths of a slender CFST square column as a function of fire exposure time calculated by the present fiber simulation technique are in excellent agreement with those given by Chung et al. [26]. In Fig. 12, P_{uo} is the ultimate axial strength of the column at ambient temperature given by Chung et al. [26]. As illustrated in Fig. 13, the evaluated fire resistances of CFST columns computed with the developed calculation procedure based on the fiber approach are in good agreement with the results obtained by the finite element model presented by Ding and Wang [30]. The fiber model generally yields slightly conservative fire-resistances of CFST columns compared to finite element results.

6. Interaction behavior of local and global buckling

The computer program implementing the numerical model was utilized to quantify the sensitivities of the interaction of local and global buckling responses of concentrically loaded slender CFST rectangular columns under fire to the tube local buckling, concrete strength, steel yield strength, member slenderness and width-to-thickness ratio of steel tube. In the parametric studies, the Young's modulus of steel at ambient temperature was 200 GPa. The initial geometric-imperfection at the mid-length of the columns was specified as $L/1000$. The details of the columns used in the parametric studies are given in Table 2.

6.1. Effects of local buckling

The local buckling effects on the global buckling behavior as well as the fire-resistance of slender CFST columns having a square section were investigated by means of using the computational program. For this investigation, the responses of the CFST columns in Group 1 given in Table 2 exposed to fire were simulated by means of considering local buckling or ignoring it, respectively. The predicted axial load-lateral displacement curves of the columns with the B/t_s ratios of 100, 80 and 60 at various fire-exposure times are presented in Figs. 14-16, respectively. It can be seen that local buckling considerably reduces the ultimate loads of CFST columns and has the most pronounced influence on the ultimate axial load of the columns at ambient temperature. As depicted in Fig. 14, the reduction in the ultimate axial load of the column caused by local buckling at exposure time of 20 min is 8%. The ultimate axial strength-fire resistance curves for the column with the B/t_s ratios of 100 are provided in Fig. 17, where P_{uo} is the ultimate axial strength of the column at ambient temperature without considering local buckling. It is found from Fig. 17 that the local buckling effect on the ultimate load decreases as the time of fire exposure increases. The reductions in the ultimate strength of the column with the B/t_s ratios of 100 caused by local buckling at fire exposure times 0 min, 20 min, 40 min and 60 min are 11%, 8%, 5% and 2%, respectively.

6.2. Effects of column slenderness ratio

The effect of the column slenderness ratio (*L/r*) on the fire behavior of CFST columns was examined by means of analyzing the slender CFST square columns in Group 2 in Table 2 by the computer program developed. The column slenderness ratios of 22, 40, 50 and 60 were determined by varying the length. The predicted global buckling responses of these columns at the fire exposure time of 20 min are given Fig. 18, It is discovered that increasing the *L*/*r* ratio results in a significant decrease in the column ultimate load but a significant increase in the

lateral displacement at the peak load. The effect of the *L*/*r* ratio on the ultimate load-fire exposure time relations of CFST square columns is illustrated in Fig. 19, where P_{uo} is the ultimate axial strength of the column with an *L*/*r* ratio of 22 at ambient temperature. At the fire exposure time of 20 min, when the *L*/*r* ratio increases from 22 to 40, 50 and 60, the column ultimate load decreases by 12 %, 23% and 35%, respectively. However, at time of 60 min, the column ultimate strength decreases by 19%, 34%, and 48%, respectively. This implies that the longer the fire exposure time, the lower the ultimate strength of the more slender column.

6.3. Effects of concrete strength

The infill concrete of the CFST columns plays a significant role in resisting the fire loading. The sensitivities of the interaction of local and global buckling responses and fire performance of rectangular CFST columns to the concrete strength were studied by using the columns in Group 3 in Table 1. Four grades of concrete strengths were used, namely 25 MPa, 35 MPa, 45 MPa and 55 MPa. The computed axial load-lateral displacement curves for these columns made of different concrete strengths are shown in Fig. 20. Both the ultimate axial load and initial stiffness of the columns are found to increase by the increase in the concrete strength. The sensitivities of the ultimate load-fire exposure time curves to the concrete strength are demonstrated in Fig. 21, where P_{uo} is the ultimate axial strength of the column with 25 MPa concrete at ambient temperature. At the ambient temperature, the column ultimate strengths are found to increase by 27%, 53% and 80%, respectively, when the concrete strength is increased from 25 MPa to 35 MPa, 45 MPa and 55 MPa. At fire time of 20 min, the increases in the ultimate strengths are 35%, 71% and 106 %, respectively. This is owing to the fact that the mechanical properties and the steel tube local buckling strength are significantly reduced by high temperatures, and the axial load is transferred from the buckled steel tube to the concrete

infill. The use of higher strength concrete leads to the higher ultimate strengths of the columns when exposed to the same fire time.

6.4. Effects of steel yield strength

The columns in Group 4 in Table 2 were analyzed by using the computer program developed to investigate the influences of steel yield stress on the interaction of local and global buckling of CFST rectangular columns exposed to fire. The predicted the interaction responses of local and global buckling of the columns at the 20 min fire exposure time are given in Fig. 22. It is apparently shown that at this level of temperatures, the steel yield stress has only minor effect on the column behavior. During the first 20 min fire exposure, the temperature on the steel tube surfaces increases significantly, which causes yielding in the steel tubes regardless of their yield strengths at room temperature. The ultimate axial strength-fire exposure time curves as a function of the yield stress of steel have been plotted in Fig. 23, where P_{uo} is the ultimate axial strength of the column with a steel yield strength of 250 MPa at ambient temperature. The steel yield stress is found to have a pronounced influence on the column ultimate load exposed to room temperature and its influence diminishes as the time of fire exposure increases. At 20 min fire exposure time, the increase in the steel yield stress from 250 MPa to 450 MPa leads to a slight increase in the column strength by 3%. This suggests that high strength steel tubes are not effective in resisting high temperatures in a fire situation.

6.5. Effects of width-to-thickness ratio

The influences of the B/t_s ratios on the interaction responses of local and global buckling of CFST square columns were investigated by means of analyzing the columns in Group 5 in

Table 2. The B/t_s ratios of 40, 60, 80 and 100 were calculated by means of varying only the tube thickness. Figure 24 presents the buckling responses of the columns with various B/t_s ratios at 20 min fire exposure time. Reducing the thickness of the tube with a B/t_s ratio less than 60 markedly decreases the column ultimate load at the exposure time of 20 min. However, for columns with a B/t_s ratio greater than 60, the effect of the tube thickness on the column ultimate strength can be neglected as indicated in Fig. 24. The ultimate load-fire exposure time relationships of the columns are demonstrated in Fig. 25, where P_{uo} is the ultimate axial strength of the column with a B/t_s ratio of 40 at ambient temperature. The B/t_s ratio is shown to have a pronounced influence on the ultimate strength of the columns exposed to room temperature. Its influence decreases with increasing the time of fire exposure. At ambient temperature, when increasing the B/t_s ratio from 40 to 100, the reduction in the ultimate strength is 24%. However, at exposure time of 20 min, the strength reduction is only 15 %. As depicted in Fig. 25, after the columns have been exposed to fire for 40 min, the effect of the B/t_s ratio on the column strength could be ignored. This is because after 40 min fire exposure, the axial load is mainly carried by the concrete core. This confirms the experimental observation which showed that the wall thickness had little effect on the fire resistance of CFST columns [13].

6.6 Effects of preloads

The computer model proposed by Kamil et al. [46] was employed to analyze the square CFST column in Group 5 in Table 2 with the preload ratios (β) of 0.0, 0.4 and 0.6 to examine the effects of the preload ratio on the column ultimate axial load. The preload ratio (β) is defined as the ratio of the applied axial load to the ultimate axial strength of the column without preload at ambient temperature. The column had the loading eccentricity ratio (e/D) of 0.1. The tensile

behavior of concrete was considered. The predicted column ultimate strength-fire exposure time curves as a function of preload ratio are presented in Fig. 26, where P_{uo} is the ultimate axial strength of the column without preload at ambient temperature. It is evident that regardless of the fire exposure time, increasing the preload ratio decreases the column ultimate strength. When the column is in room temperature, increasing the preload ratio from 0.0 to 0.4 and 0.6 leads to a reduction in the column strength by 4% and 6%, respectively. As depicted in Fig. 26, the column has the most pronounced strength reduction at the fire exposure time of 20 min. At this time, the reductions in the column strength were obtained as 12% and 21%, respectively, when changing the preload ratio from 0.0 to 0.4 and 0.6. At the fire-exposure time of 60 min, increasing the preload ratio from 0.0 to 0.6 leads to a reduction in the column strength by 16%.

7. Conclusions

The computational model formulated by the fiber approach has been presented in this paper for predicting the fire-resistance and the interaction behavior of local and global buckling in concentrically-loaded slender rectangular CFST subjected to fire loading. The model has taken into account important features, including the interaction of local and global buckling, air gap between the concrete and steel tube, water contents in concrete, emissivity of exposed surfaces, temperature-dependent material and geometric nonlinearities, initial geometric imperfections and preloads in the simulation. The verified numerical model has been utilized to investigate the interaction behavior of local and global buckling of CFST columns exposed to standard fire, and can be used in the structural fire engineering design of such composite columns.

The concluding remarks are given as follows:

(1) The fiber-based computational model proposed can predict the fire-resistances of CFST rectangular columns with reasonable accuracy compared to standard-fire test and numerical results available in the literature.

(2) The effect of the tube local buckling on the column ultimate axial strength decreases as the fire exposure time increases. At ambient temperature, local buckling may reduce the ultimate load of the CFST column with a B/t_s ratio of 100 by 11%, but at the fire-exposure time of 20 min, the reduction is 8%.

(3) The ultimate axial resistance of CFST columns exposed to fire reduces significantly when the member slenderness increases. This effect increases as the time of fire exposure increases. The ultimate strength of the column with an *L/r* ratio of 60 at the fire-exposure time of 60 min may reduce by 48% compared to the that of the column with an *L/r* ratio of 22.

(4) Significant increases in the ultimate load of CFST columns are obtained by using higher strength concrete at any fire-exposure time. At the fire-exposure time of 20 min, the percentage increase in the column ultimate load could be 106% by increasing the concrete strength from 25 MPa to 55 MPa.

(5) The yield stress of steels has a minor influence on the column ultimate load at elevated temperatures. At the fire-exposure time of 20 min, increasing the steel yield strength from 250 MPa to 450 MPa leads to only 3% improvement in the column strength.

(6) At ambient temperature, the B/t_s ratio has a considerable influence on the column ultimate resistance, but its influence decreases when the fire-exposure time increases. After 40 min fire exposure, this effect could be ignored.

(7) Increasing the preload ratio generally decreases the ultimate strength and fire-resistance of slender CFST columns. For columns subjected to a preload ratio of 0.6, the reduction in the ultimate load could be up to 21%.

The advantages of the developed fiber-based computational model are its simplicity in mathematical formulation, computational efficiency, and its ability in simulating the interaction behavior of local and global buckling. Its disadvantage is that the equilibrium is maintained only at the column mid-height. The fiber-based computational model proposed has incorporated important features, such as the interaction of local and global buckling, deflections caused by preloads and initial geometric imperfections, which have not been considered in the fiber-based models proposed by other researchers [22-29]. The fiber-based numerical model developed is computationally more efficient than the 3D finite element models presented by other researchers [30-32].

References

[1] L.H. Han, W. Li, R. Bjorhovde, Developments and advanced applications of concrete-filled steel tubular (CFST) structures: Members, J. Constr. Steel Res. 100 (2014) 211-228.

[2] J.F. Hajjar, P.H. Schiller, A. Molodan, A distributed plasticity model for concrete-filled steel tube beam-columns with interlayer slip, Eng. Struct. 20(8) (1998) 663-676.

[3] K.A.S. Susantha, H.B. Ge, T. Usami, Uniaxial stress-strain relationship of concrete confined by various shaped steel tubes, Eng. Struct. 23(10) (2001) 1331-1347.

[4] N.E. Shanmugam, B. Lakshmi, B. Uy, An analytical model for thin-walled steel box columns with concrete in-fill, Eng. Struct. 24(6) (2002) 825-838.

[5] Q.Q. Liang, Performance-based analysis of concrete-filled steel tubular beam-columns. Part I: Theory and algorithms, J. Constr. Steel Res. 65(2) (2009) 363-373.

[6] Q.Q. Liang, V.I. Patel, M.N.S. Hadi, Biaxially loaded high-strength concrete-filled steel tubular slender beam-columns. Part I: Multiscale simulation, J. Constr. Steel Res. 75 (2012) 64-71.

[7] M.H. Mollazadeh, Y.C. Wang, New insights into the mechanism of load introduction into concrete-filled steel tubular column through shear connection, Eng. Struct. 75 (2014) 139-151.

[8] M.X. Xiong, D.X. Xiong, J.Y.R. Liew, Axial performance of short concrete filled steel tubes with high-and ultra-high-strength materials, Eng. Struct. 136 (2017) 494-510.

[9] AS 3600-2009, Australian Standard for Concrete structures, Standards Australia, Sydney, NSW, Australia, 2009.

[10] Y.C. Wang, Steel and Composite Structures: Behaviour and Design for Fire Safety, London and New York: Spon Press, 2002.

[11] Q.Q. Liang, Analysis and Design of Steel and Composite Structures, CRC Press, Taylor and Francis Group, Boca Raton and London, 2014.

[12] G.M. Kamil, Q.Q. Liang, M.N.S. Hadi, Numerical analysis of axially loaded rectangular concrete-filled steel tubular short columns at elevated temperatures, Eng. Struct. 180 (2019) 89-102.

[13] T.T. Lie, M. Chabot, Experimental studies on the fire resistance of hollow steel columns filled with plain concrete, Internal report, National Research Council Canada, Institute for Research in Construction, 1992-01.

[14] Y. Sakumoto, T. Okada, M. Yoshida, S. Tasaka, Fire resistance of concrete-filled, fire-resistant steel-tube columns, J. Mat. in Civil Eng. ASCE, 69(2) (1994) 169-184.

[15] V.K.R. Kodur, T.T. Lie, Fire performance of concrete-filled hollow steel columns, J. Fire Prot. Eng. 79(3) (1995) 89-98.

[16] L.H. Han, Y.F. Yang, L. Xu, An experimental study and calculation on the fire resistance of concrete-filled SHS and RHS columns, J. Constr. Steel Res. 59 (2003) 427-452.

[17] D.K. Kim, S.M. Choi, J.H. Kim, K.S. Chung, S.H. Park, Experimental study on fire resistance of concrete-filled steel tube column under constant axial loads, Int. J. Steel Struct. 5(4) (2005) 305-313.

[18] A. Espinos, M.L. Romero, E. Serra, A. Hospitaler, Circular and square slender concrete-filled tubular columns under large eccentricities and fire, J. Constr. Steel Res. 110 (2015) 90-100.

[19] A. Espinos, M.L. Romero, E. Serra, A. Hospitaler, Experimental investigation on the fire behavior of rectangular and elliptical slender concrete-filled tubular columns, Thin-Walled Struct. 93 (2015) 137-148.

[20] L.H. Han, F. Chen, F.Y. Liao, Z. Tao, B. Uy, Fire performance of concrete filled stainless steel tubular columns, Eng. Struct. 56 (2013) 165-181.

[21] Y.F. Yang, L. Zhang, X. Dai, Performance of recycled aggregate concrete-filled square steel tubular columns exposed to fire, Adv. in Struct. Eng. 20(9) (2017) 1340-1356.

[22] T.T. Lie, M. Chabot, A method to predict the fire resistance of circular concrete filled hollow steel columns, J. Fire Prot. Eng. 2(4) (1990) 111-126.

[23] T.T. Lie, R.J. Irwin, Fire resistance of rectangular steel columns filled with bar-reinforced concrete, J. Struct. Eng. ASCE, 12(5) (1995) 797-805.

[24] L.H. Han, Fire performance of concrete filled steel tubular beam-columns, J. Constr. Steel Res. 57 (2001) 695-709.

[25] K. Chung, S. Park, S. Choi, Material effect for predicting the fire resistance of concrete-filled square steel tube column under constant axial load, J. Constr. Steel Res. 64 (2008) 1505-1515.

[26] K. Chung, S. Park, S. Choi, Fire resistance of concrete filled square steel tube columns subjected to eccentric axial load, Int. J. Steel Struct. 9 (2009) 69-76.

[27] C. Renaud, J.M. Aribert, B. Zhao, Advanced numerical model for the fire behavior of composite columns with hollow steel section, Steel and Compo. Struct. 3(2) (2003) 75-95.

[28] H. Yang, L.H. Han, Y.C. Wang, Effects of heating and loading histories on post-fire cooling behaviour of concrete-filled steel tubular columns, J. Constr. Steel Res. 54 (2008) 556-570.

[29] C. Ibañez, M.L. Romero, A. Hospitaler, Fiber beam model for fire response simulation of axially loaded concrete filled tubular columns, Eng. Struct. 56 (2013) 182-193.

[30] J. Ding, Y.C. Wang, Realistic modelling of thermal and structural behaviour of unprotected concrete filled tubular columns in fire, J. Constr. Steel Res. 64 (2008) 1086-1102.

[31] A. Espinos, M.L. Romero, A. Hospitaler, Advanced model for predicting the fire response of concrete filled tubular columns, J. Constr. Steel Res. 66 (2010) 1030-1046.

[32] S.D. Hong, A.H. Varma, Analytical modeling of the standard fire behavior of loaded CFT columns, J. Constr. Steel Res. 65 (2009) 54-69.

[33] Q.Q. Liang, Numerical simulation of high strength circular double-skin concrete-filled steel tubular slender columns, Eng. Struct. 168 (2018) 205-217.

[34] Eurocode 1. 1991-1-2, Actions on structures, Part 1.2: General actions- Actions on structures exposed to fire, CEN, Brussels, Belgium, 2002.

[35] F.P. Incropera, D.P. Dewitt, T.L. Bergman, A.S. Lavine, Fundamentals of heat and mass transfer, John Wiley & Sons, 6th Edition, USA 2005.

[36] Eurocode 3. Design of steel structures, Part 1.2: General rules-structural fire design, CEN, Brussels, Belgium, 2005.

[37] Eurocode 2. Design of concrete structures, Part 1.2: General rules-structural fire design, CEN, Brussels, Belgium, 2004.

[38] M.X. Xiong, Y.H. Wang, J.Y.R. Liew, Evaluation on thermal behaviour of concrete-filled steel tubular columns based on modified finite difference method, Adv. in Struct. Eng. 19(5) (2016) 746-761.

[39] G.M. Kamil, Q.Q. Liang, M.N.S. Hadi, Local buckling of steel plates in concrete-filled steel tubular columns at elevated temperatures, Eng. Struct. 168 (2018) 108-118.

[40] Q.Q. Liang, B. Uy, J.Y.R. Liew, Local buckling of steel plates in concrete-filled thin-walled steel tubular beam-columns, J. Constr. Steel Res. 63(3) (2007) 396-405.

[41] H. Shakir-Khalil, J. Zeghiche, Experimental behaviour of concrete-filled rolled rectangular hollow-section columns, The Struct. Engr. 67(19) (1989) 346–53.

[42] Q.Q. Liang, High strength circular concrete-filled steel tubular slender beam-columns, Part I: Numerical analysis, J. Constr. Steel Res. 67(2) (2011) 164-171.

[43] V.I. Patel, Q.Q. Liang, M.N.S. Hadi, High strength thin-walled rectangular concrete-filled steel tubular slender beam-columns. Part I: Modeling, J. Constr. Steel Res. 70 (2012) 377-384.

[44] V.I. Patel, Q.Q. Liang, M.N.S. Hadi, Behavior of biaxially-loaded rectangular concrete-filled steel tubular slender beam-columns with preload effects, Thin-Walled Struct. 79 (2014) 166-177.

[45] D.E. Müller, A method for solving algebraic equations using an automatic computer, MTAC 1956; 10:208-15.

[46] G.M. Kamil, Q.Q. Liang, M.N.S. Hadi, Fire-resistance of eccentrically loaded rectangular concrete-filled steel tubular slender columns incorporating interaction of local and global buckling, Int. J. Struct. Stab. Dyn. 19(8) (2019) 1950085.

Figures and Tables

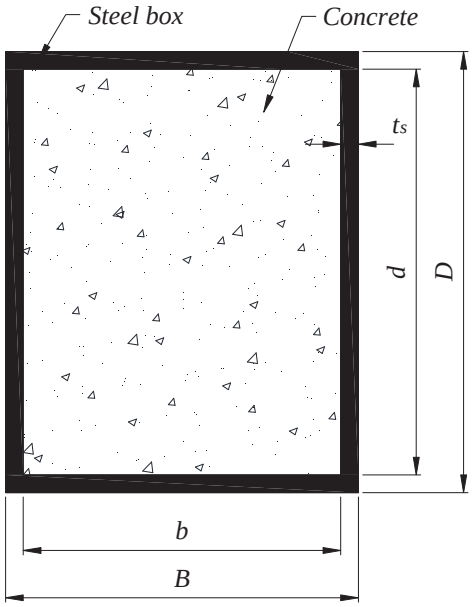

Fig. 1. Cross-section of rectangular CFST column.

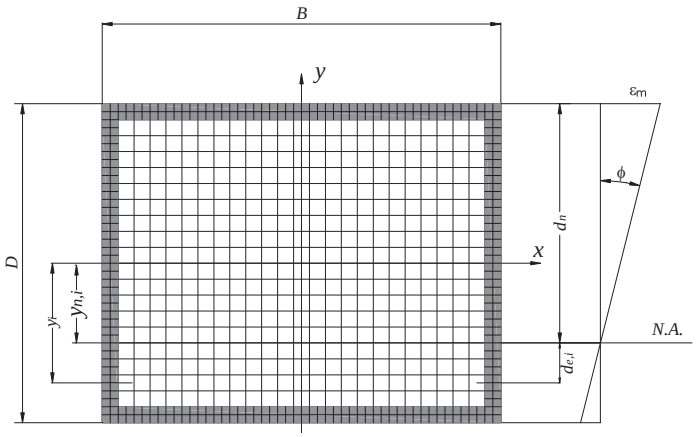

Fig. 2. Typical fiber mesh and strain distribution in a rectangular column cross-section

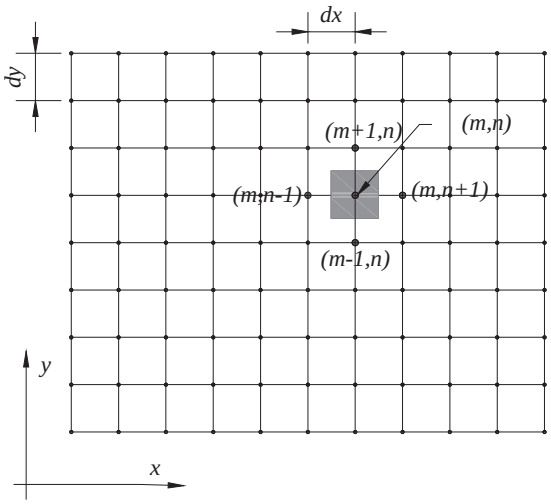

Fig. 3. Nodal grid for the temperature calculations using the method of finite differences

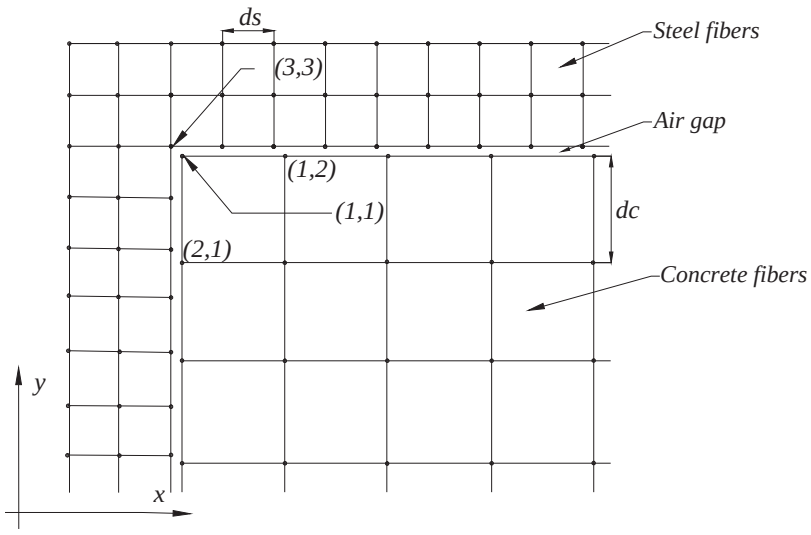

Fig. 4. Typical nodal grids for the interface of steel and concrete for the finite difference temperature analysis

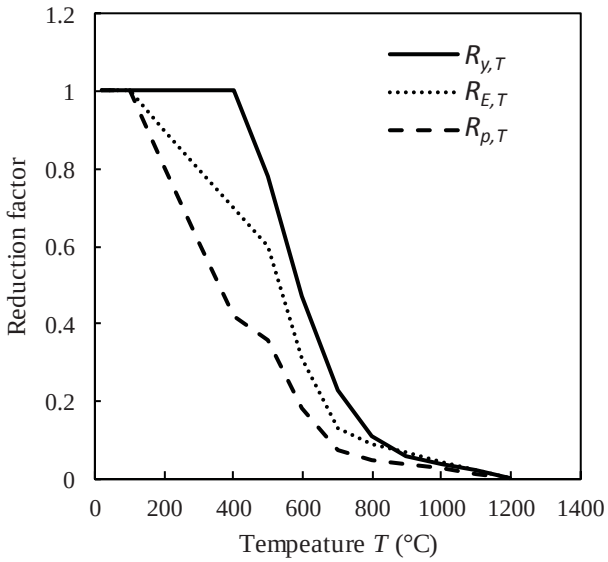

Fig. 5. Reduction factors for the mechanical properties of structural steels at elevated temperatures based on Eurocode 3 [36].

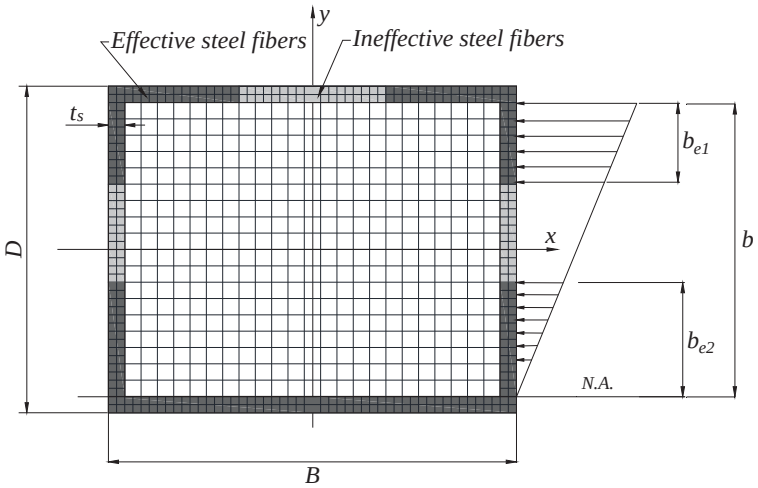

Fig. 6. Effective and ineffective widths of steel tube walls in rectangular CFST column section under uniaxial bending

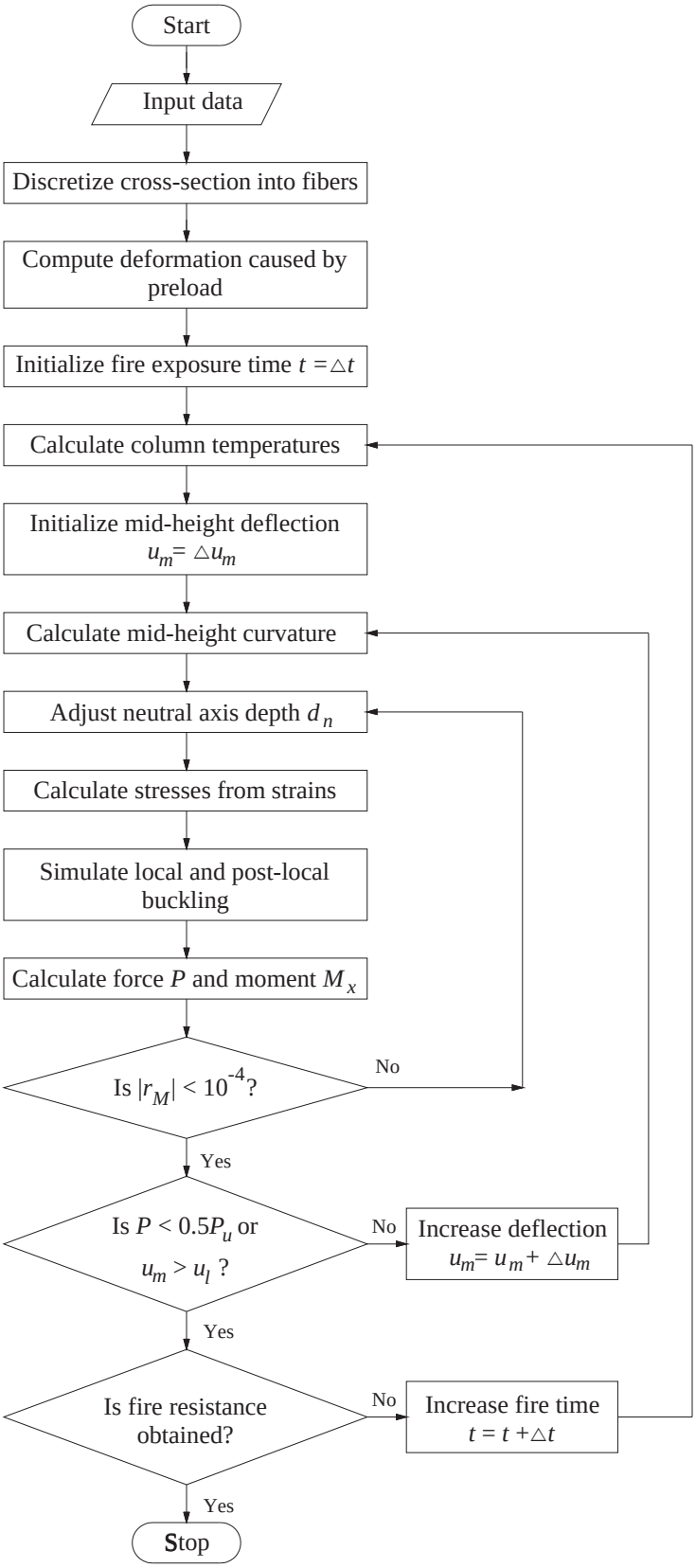

Fig. 7. Computer flow chart for calculating the fire resistance of axially loaded rectangular CFST slender columns exposed to fire

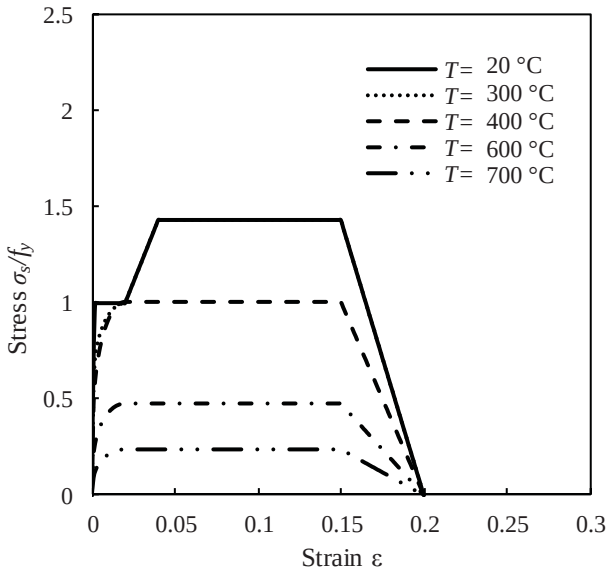

Fig. 8. Stress-strain curves for structural steels at elevated temperatures allowing for strain hardening based on Eurocode 3 [36].

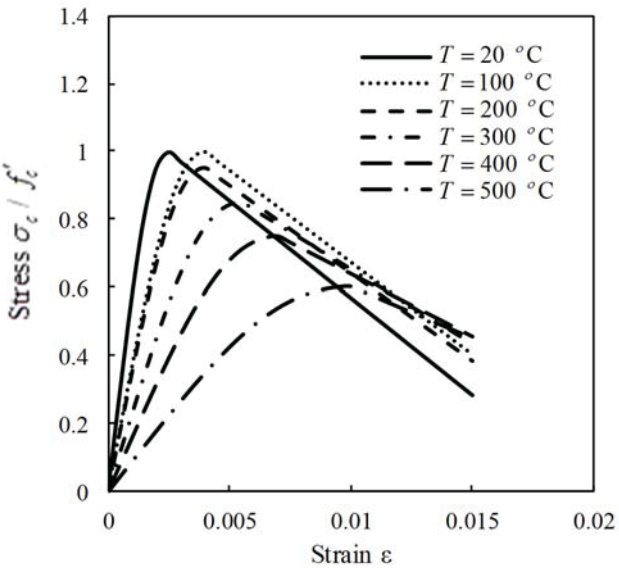

Fig 9. Stress-strain curves for concrete at elevated temperatures based on Eurocode 2 [37].

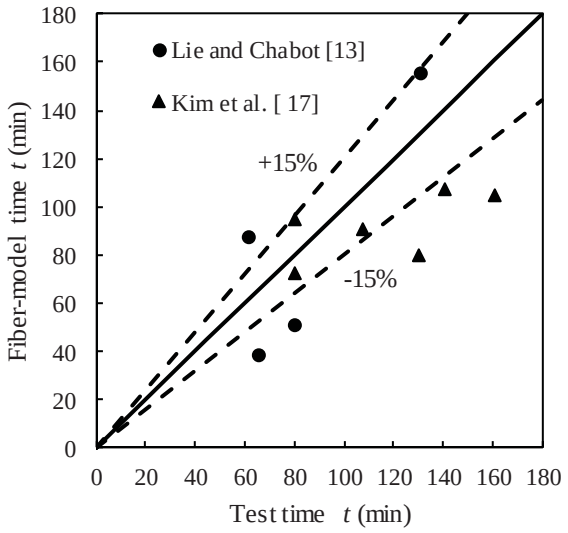

Fig. 10. Comparison of predicted fire-resistances of slender square CFST columns with test results given by Lie and Chabot [13] and Kim et al. [17].

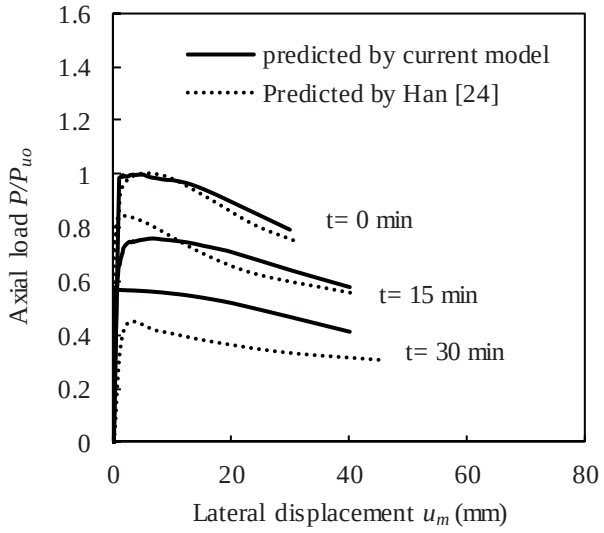

Fig. 11. Comparison of the axial load-lateral displacement curves for a square CFST columns in fire computed by the proposed computational model and the model by Han [24].

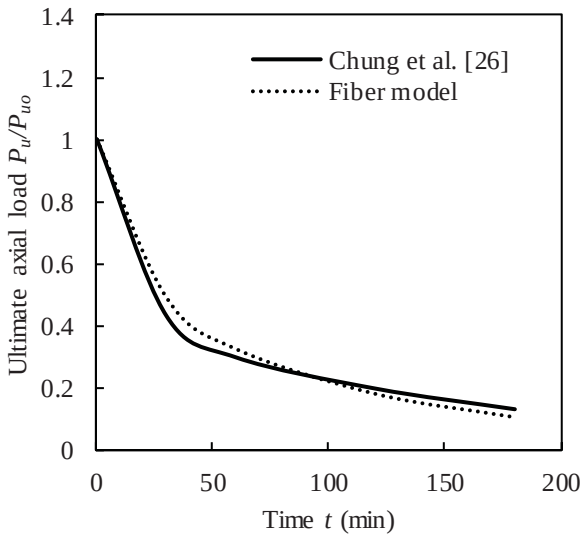

Fig. 12. Comparison of the ultimate strength-fire exposure time curves for a square CFST column calculated by the proposed fiber model and the model by Chung et al. [26].

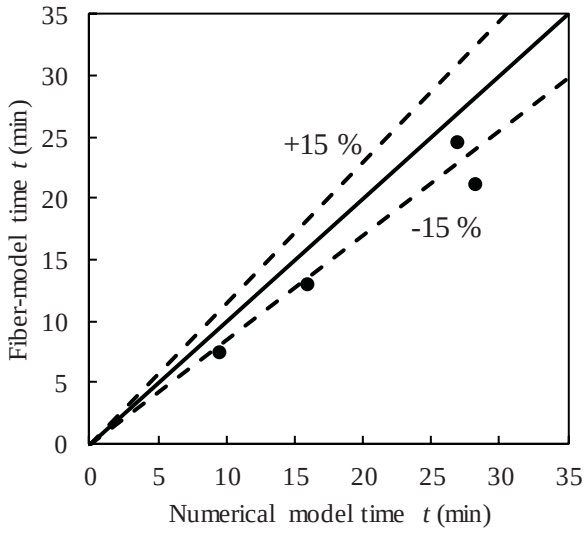

Fig. 13. Comparison of fire-resistances of CFST columns predicted by the proposed fiber-based computational model with the finite element results given by Ding and Wang [30].

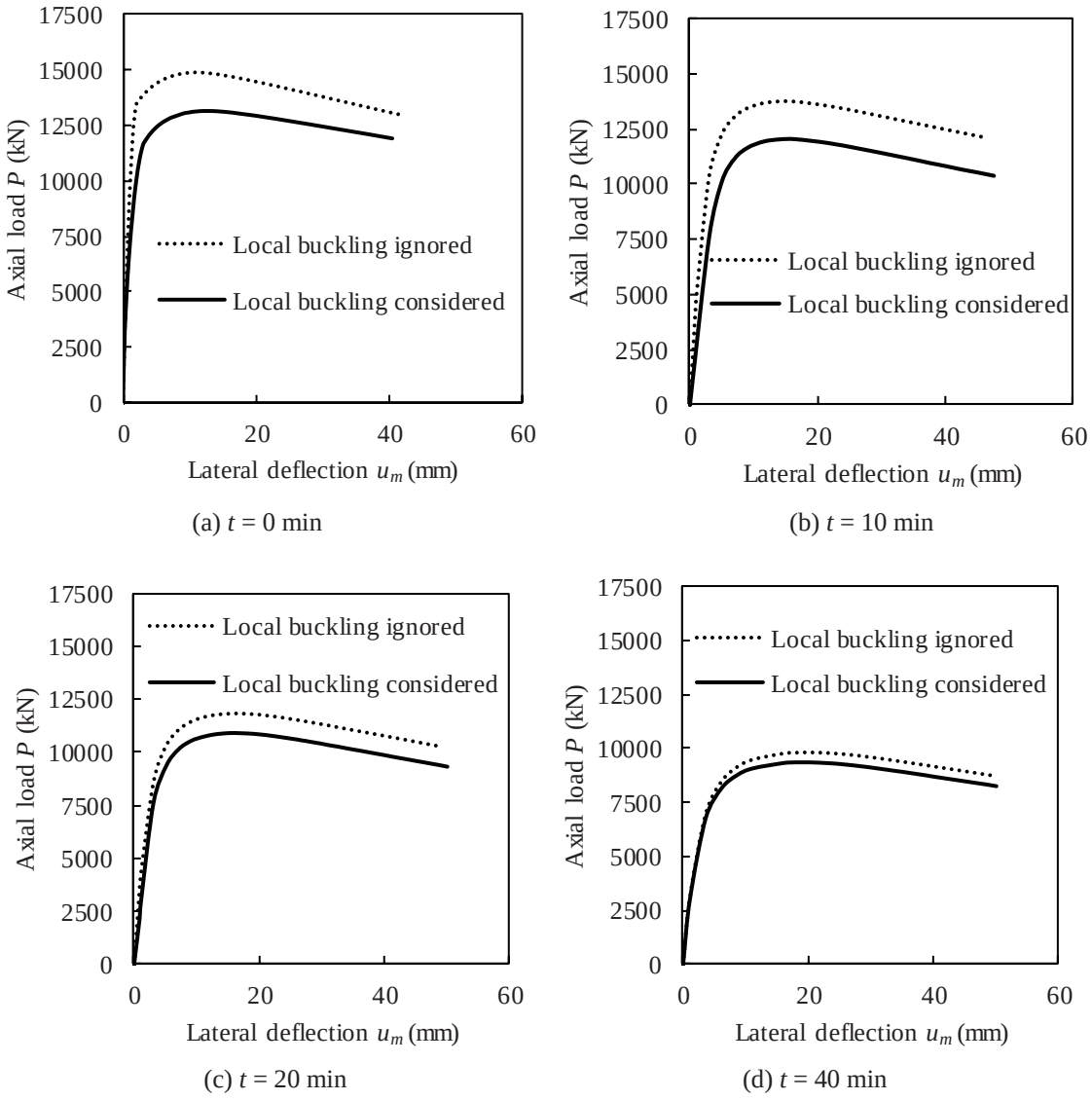

Fig. 14. Influences of local buckling on the axial load-lateral deflection curves of slender square CFST column with the B/t_s ratio of 100 at various fire-exposure time.

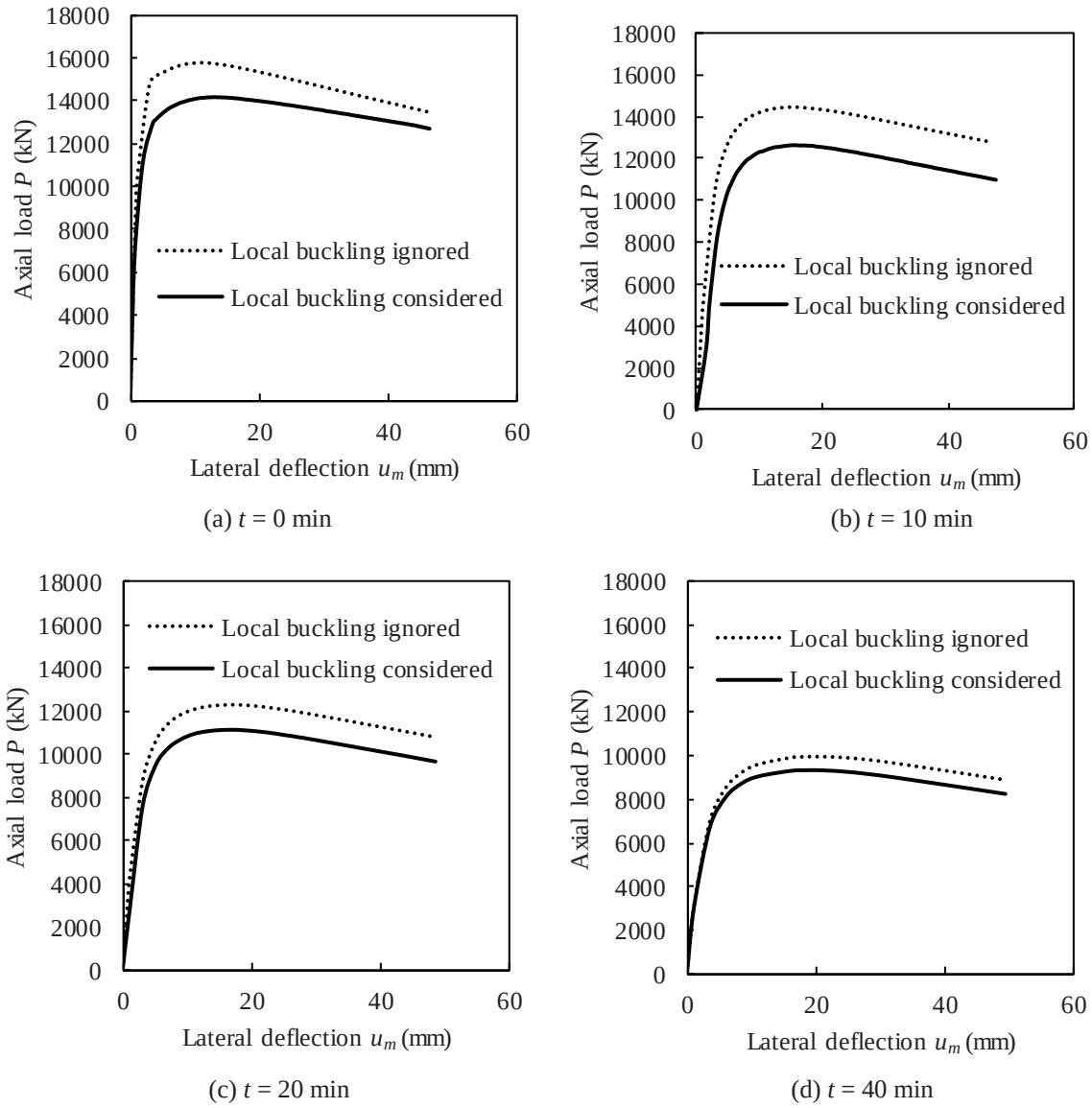

Fig. 15. Influences of local buckling on the axial load-lateral deflection behavior of slender square CFST column with the B/t_s of 80 at various fire-exposure time.

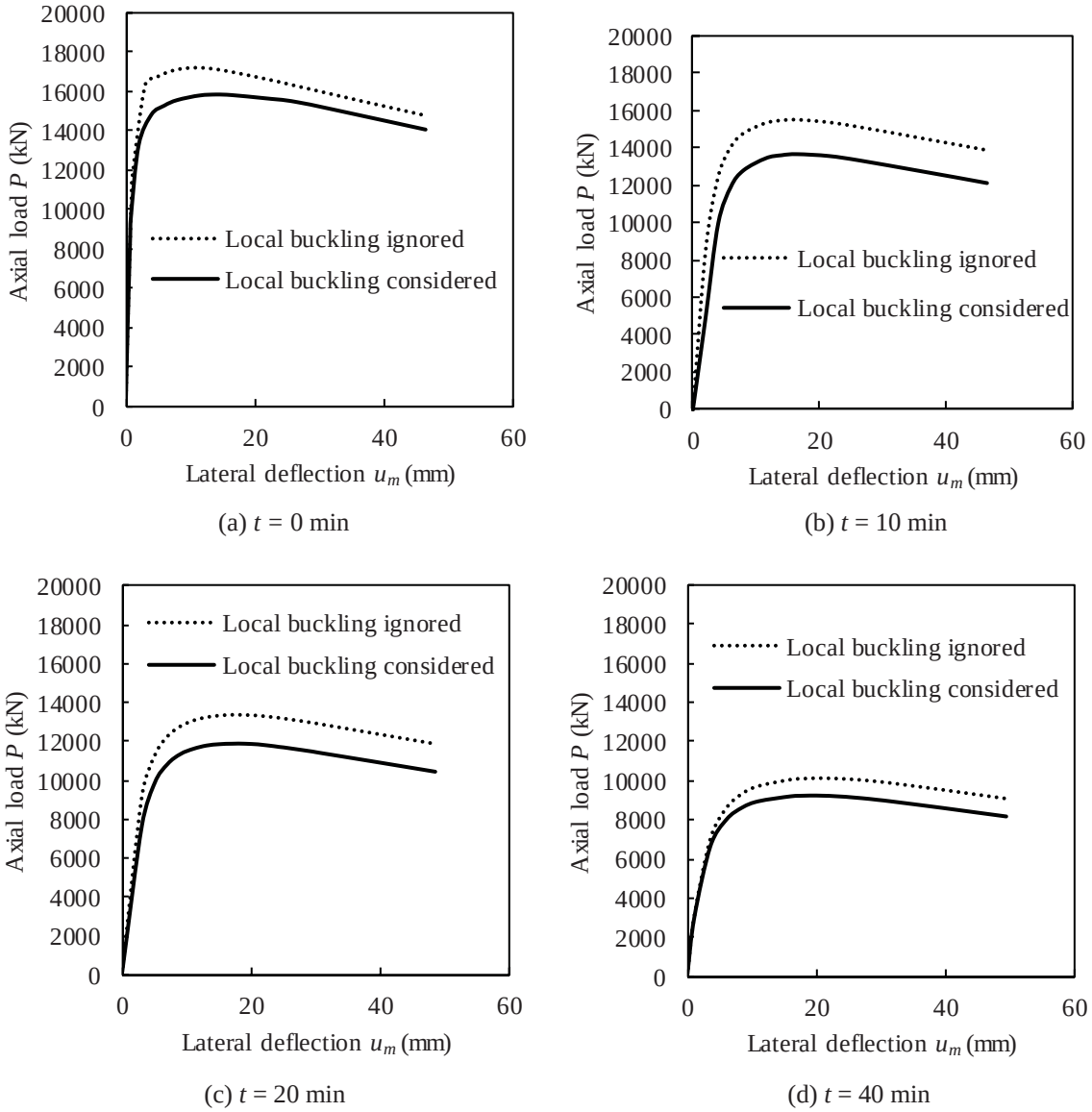

Fig. 16. Influences of local buckling on the axial load-lateral deflection behavior of slender square CFST column with the B/t_s of 60 at various fire-exposure time.

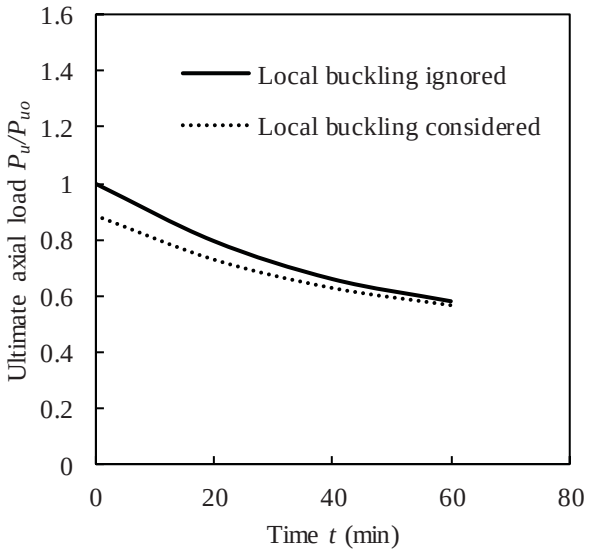

Fig. 17. Influences of local buckling on the ultimate axial strength-fire exposure time curve for slender CFST column with the B/t_s ratio of 100.

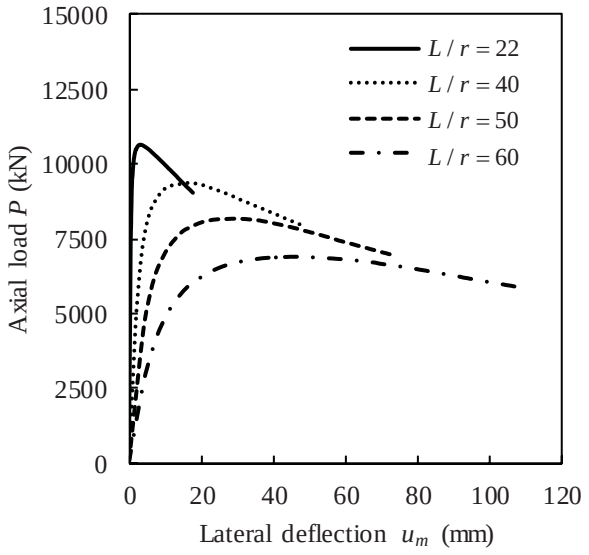

Fig. 18. Axial load-lateral displacement curves of square slender CFST columns with various slenderness ratio at fire-exposure time of 20 min.

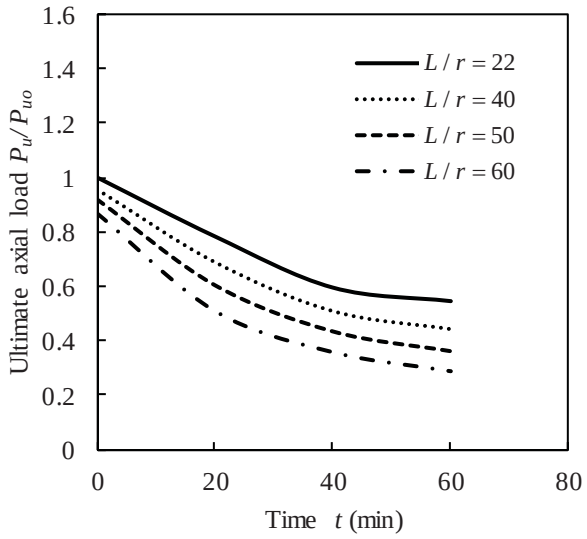

Fig. 19. Effects of the column slenderness ratio on the ultimate strength-fire exposure time curves of square slender CFST columns.

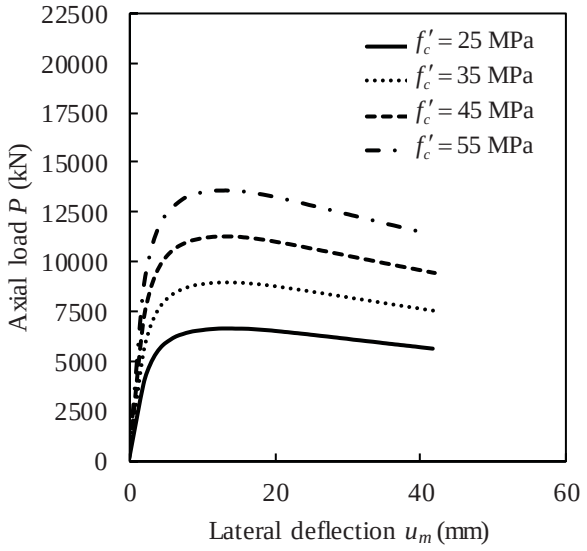

Fig. 20. Axial load-lateral displacement curves of rectangular slender CFST columns with various concrete strengths at fire-exposure time of 20 min

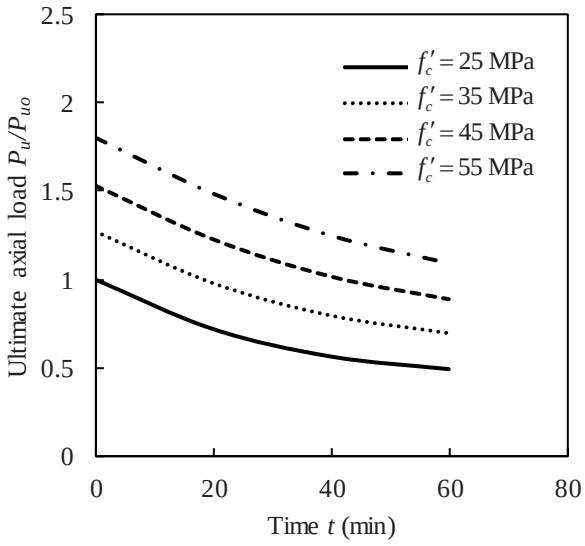

Fig. 21. Effects of the concrete strength on the ultimate strength-fire exposure time curves of rectangular slender CFST columns.

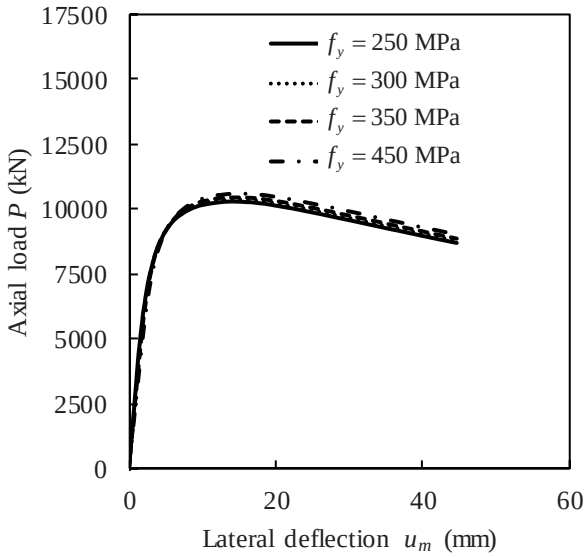

Fig. 22. Axial load-lateral displacement curves of rectangular slender CFST columns with different yield strengths at fire-exposure time of 20 min

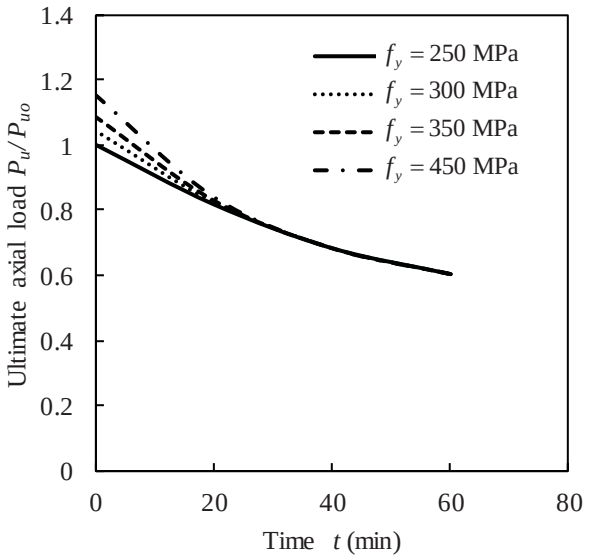

Fig. 23. Effects of the steel yield strength on the ultimate strength-fire exposure time curves of rectangular slender CFST columns.

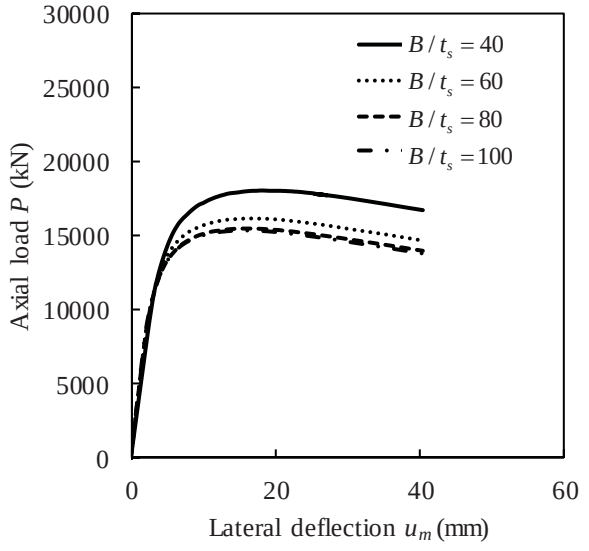

Fig. 24. Axial load-lateral displacement curves of square slender CFST columns with various B/t_s ratios at fire-exposure time of 20 min

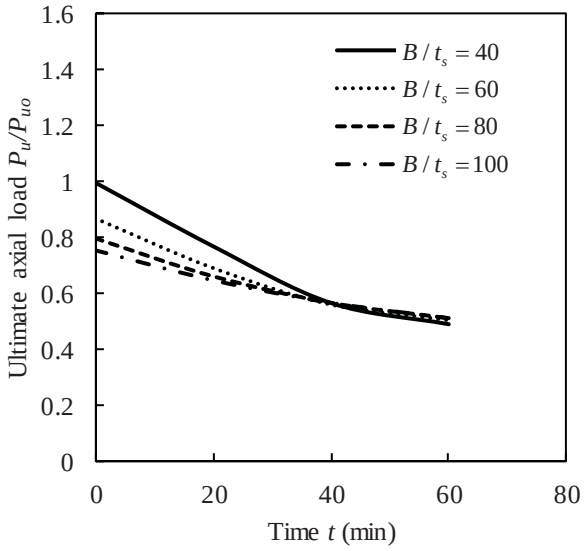

Fig. 25. Effects of B/t_s ratios on the ultimate strength-fire exposure time curves of square slender CFST columns.

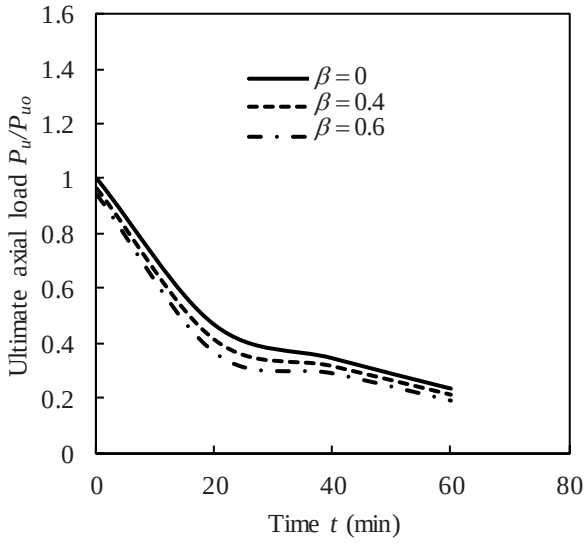

Fig. 26. Effects of preload ratios on the column strength-fire exposure time curves.

Table 1. Dimensions and properties of CFST slender columns used in the verifications

Specimen	$B\times D\times t_s$ (mm)	B/t_s	L (mm)	L/r	f_y (MPa)	$f_c^{'}$ (MPa)	P (kN)	Measured t (min)	Computed t (min)	Diff. (%)	Ref.
SQ-01	152.4×152.4×6.35	24	1905	43.3	350	58.3	376	66	38.8	41.2	[13]
SQ-7	177.8×177.8×6.35	28	1905	37.1	350	57	549	80	51.025	36.2	
SQ-17	254×254×6.35	40	1905	26	350	58.3	1096	62	87.7	41.5	
SQ-24	304.8×304.8×6.35	48	1905	21.7	350	58.8	1130	131	155	18.3	
SAL1	300×300×9	33.3	3500	40.4	363	27.5	842.8	80.2	72.81	9.2	[17]
SAL2	300×300×9	33.3	3500	40.4	363	27.5	744.8	130.4	80	38.7	
SAH1	300×300×9	33.3	3500	40.4	363	37.8	1401.4	44.4	65.6	47.7	
SBL1	350×350×9	38.9	3500	34.6	363	27.5	1293.6	80.3	95	18.3	
SBL2	350×350×9	38.9	3500	34.6	363	27.5	1038.8	160.6	105	34.6	
SBH1	350×350×9	38.9	3500	34.6	363	37.8	1940.4	107.9	90.9	15.8	
SBH2	350×350×9	38.9	3500	34.6	363	37.8	1558.2	140.6	107.4	23.6	
A1b	200×100×5	40	3000	52	275	30	268	15.84	13.07	17.5	[30]
B1b	200×200×6.3	31.7	3000	52	275	30	660	26.86	24.7	8	
C1b	200×200×12.5	16	3000	52	275	30	969	28.16	21.16	24.9	
C3b	200×200×12.5	16	3000	52	275	30	2261	9.45	7.53	20.3	
SC1	400×400×12	33.3	4000	34.6	345	50	-	-	-	-	[24]
SC2	350×350×9	38.9	3000	29.7	363	27.5	-	-	-	-	[26]
Mean										26.4	
Standard deviation (SD)										194.4	
Coefficient of variation (COV)										7.4	

Table 2. Dimensions and properties of CFST slender columns used in the parametric studies

Group	Column	B×D (mm)	B/t_s	L/r	$f_c^{'}$ (MPa)	f_y (MPa)
1	C1	600×600	100	40	35	300
	C2	600×600	80	40	35	300
	C3	600×600	60	40	35	300
2	C5	500×500	50	22	40	300
	C6	500×500	50	40	40	300
	C7	500×500	50	50	40	300
	C8	500×500	50	60	40	300
3	C9	450×650	64.5	40	25	300
	C10	450×650	64.5	40	35	300
	C11	450×650	64.5	40	45	300
	C12	450×650	64.5	40	55	300
4	C13	500×600	71.4	40	40	250
	C14	500×600	71.4	40	40	300
	C15	500×600	71.4	40	40	350
	C16	500×600	71.4	40	40	450
5	C17	600×600	40	40	50	300
	C18	600×600	60	40	50	300
	C19	600×600	80	40	50	300
	C20	600×600	100	40	50	300
6	C21	400×400	80	60	45	350